Destabilization and Dry-Spot Nucleation in Thin Liquid Films on Partially Wetting Substrates using a Low-Pressure Air-Jet

Christian W.J. BERENDSEN, Jos C.H. ZEEGERS, Anton A. DARHUBER[*]

* Corresponding author: Fax: +31 (0)40 243 8272; Email: a.a.darhuber@tue.nl
Mesoscopic Transport Phenomena Group, Department of Applied Physics, Eindhoven University of Technology, NL

Abstract The rupture of a thin liquid film on a partially wetting substrate can be initiated by external forces. In this manuscript we present experiments and numerical simulations of the effects of a laminar axisymmetric air-jet impinging on triethylene glycol films. We numerically calculate stagnation pressures and shear stress distributions that are used in a model for the thin liquid film dynamics. Experimentally, we distinguish three regimes: 1) the depressions made by low pressure air-jets level out, 2) for intermediate pressures a single dry-spot is nucleated that grows with a constant dewetting speed, whereas 3) for higher pressure air-jets the film is thinned and a large number of dry-spots nucleate, grow and leave a droplet pattern behind. In the third regime the dewetting speed was not independent of local film thickness. Numerical simulations show a qualitative agreement with the experimental observations.

Keywords: Thin Film Rupture, Dewetting, Disjoining Pressure, Partial Wetting, Impinging Jet

1. Introduction

A thin liquid film on a partially wetting substrate can be intrinsically unstable and/or destabilized by external forces (Sharma and Ruckenstein 1986). Upon film rupture, dry spots nucleate that grow and coalesce. Patterns of small droplets appear where the liquid rims surrounding the dry spots meet (Reiter 1992). This - usually unwanted - phenomenon is encountered in biomedical conditions (Holly 1973) and industrial applications like coating processes (Bower 2007) or immersion lithography (Streefkerk 2006).

The nucleation of a dry-spot can be induced or accelerated when the liquid film is locally thinned. This thinning can be achieved by the impingement of a gas jet on the liquid-air interface. The impact of an air-jet on deep (Collins 1954, Banks 1962 and Fagela-Alabastro 1967) or shallow liquid layers (Tuck 1983, Ellen 1984 and Lacanette 2006) has been described earlier. Moreover, air-jets have been used to induce layer breakup in studies of dewetting (Taylor 1973 and Redon 1991).

In this paper, we study the influence of a low pressure air-jet on the stability of a non-volatile thin liquid film. We develop a numerical model for the time evolution of a non-volatile thin liquid film on a partially wetting substrate using a phenomenological disjoining-pressure term to account for partial wettability. The stagnation pressure and shear stress acting on the thin film were obtained by numerical evaluation of an incompressible Navier-Stokes model of the air-jet.

For our experiments we have selected triethylene glycol, a non-volatile liquid with a relatively low receding contact angle and relatively high viscosity, such that spontaneous breakup is delayed and metastable films can be prepared that allow external triggering of breakup within a convenient timescale.

2. Experiments
2.1. Sample preparation

Thin films of triethylene glycol (3EG) (Fluka 90390, purity ≥99%) are spincoated on wetting and non-wetting substrates and subjected to a laminar air-jet. The wetting samples are $50 \times 75 \, \text{mm}^2$ plain microscope slides (Corning), cleaned in piranha solution ($H_2SO_4 : H_2O_2$, 3:1 v/v), rinsed thoroughly with deionized water, blown dry using filtered air and subjected to a UV/Ozone treatment (Jelight) for 300s before use. The partially wetting samples are $60 \times 60 \, \text{mm}^2$ squares of polymethylmethacrylate (PMMA). The polymer is flushed with isopropanol and blown dry using filtered air.

Then the center of the sample is covered with an aluminium mask (30x30mm^2) and subjected to UV/Ozone treatment for 300s before use. This treatment renders the perimeter of the PMMA substrate completely wetting, while maintaining the central area partially wetting for 3EG.

The advancing and receding contact angles are measured by placing a droplet of 3EG on the PMMA surface and slowly increasing and subsequently decreasing the droplet volume. The droplet profile is imaged using a CCD camera and a telecentric lens and analyzed using ImageJ. The measured contact angles were θ_{adv}=59° and θ_{rec}=33°. Using a Pt Wilhelmy plate and an analytical balance, the surface tension of 3EG was measured to be 45.4 mN/m.

The liquid film is applied by spin coating on a Cee200 spincoater (Brewer Science) at 3000rpm for 10s. Liquid film thickness was measured by spectral interference (Fogt 1998) using a home-built setup consisting of a tungsten halogen light source and a fiber optic spectrometer (OceanOptics). A refractive index value of n=1.456 (Fluka 90390 datasheet) is used, neglecting any water content in the film. The film thickness at the center of the substrate just after spincoating was measured to be 5.9-6.0 μm both on glass and PMMA. We have, however observed a rise in the thickness (up to several μm) of the film during the course of air-jet measurements. We attribute this rise to a redistribution of the liquid rim formed at the substrate edges during spincoating.
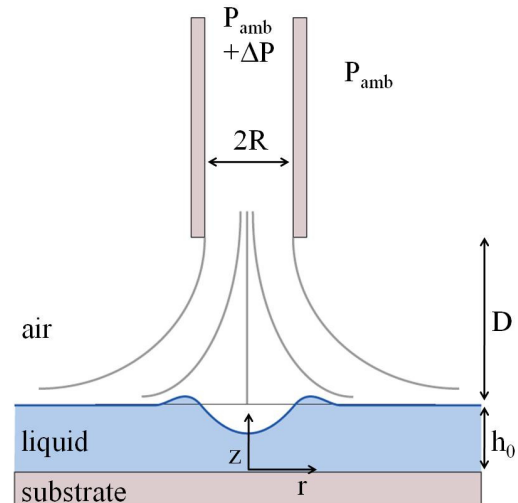
2.2. Air-jet configuration
The air-jet is generated by a setup consisting of a cylinder of pressurized air (Linde) connected through a reduction valve and a precision air pressure regulator (Negretti & Zambra) to a solenoid valve. The pressure is measured using a digital manometer (Keller LEO2). The solenoid valve is fitted with a hollow needle with an inner diameter of 2R=200 μm. The distance D between the needle and the sample can be adjusted using a translation stage. The air-jet experiments were performed at room temperature (T=19±1°C),

ambient pressure (p=103±2kPa) and relative humidity of 30±5%.

2.3 Interference microscopy
Evaluation of the height profile of the thin liquid film on the transparent solid substrate is done using optical interferometry. The imaging optics (Infinitube) fitted with a microscope objective (Olympus, MPlanAPO 2.5x/NA0.08) is positioned on a z-stage below the sample. The light source is a high power LED (640nm, Luxeon I) and 650nm long-pass filter. A CCD camera (Guppy, Applied Vision Technology) captures the microscope images. The solenoid valve and camera are controlled using a PXI computer and LabView software (National Instruments).


Figure 1: *Schematic representation of the experimental configuration (not to scale).*

3. Numerical model calculations
We are using a combined approach to model the effects of a laminar air-jet on a liquid film. The low pressure air-jet is modeled using an axisymmetric incompressible Navier-Stokes solver. Those results are used as boundary conditions for a model of the thin film dynamics, based on the lubrication equation. Figure 1 shows a schematic representation of the experimental configuration. The air-jet is generated by applying a pressure difference ΔP over a hollow needle with inner diameter 2R, positioned at a distance D from the air-liquid interface of a film with thickness h_0.

3.1 Air-jet simulations

The air-jet is modeled using the axisymmetric incompressible Navier-Stokes solver, implemented in COMSOL 3.5a, a valid approach for small Mach numbers (Ma<0.3). The numerical domain configuration is shown in Fig. 2. It includes a cavity around the needle inlet, the hollow needle, a solid plate at the position of the sample and the surrounding air space.
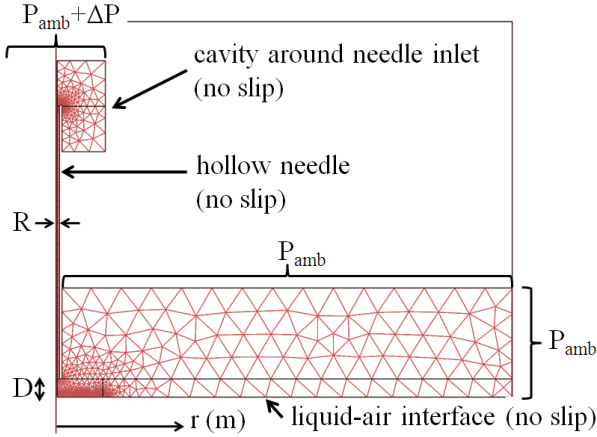
Figure 2: *The geometry and mesh used for the air-jet simulation.*

Air viscosity	μ	$1.78 \ 10^{-5}$ Pa·s
Air density	ρ	1.23 kg/m^3
Needle-plate distance	D	0.8 mm
Needle inner radius	R	100 μm

Table 1: *Parameter values used for the numerical simulation of the air-jet.*

The input pressure $P_{amb}+\Delta P$ was applied at the inlet of a cavity around the upper end of the hollow needle, while the ambient pressure P_{amb} was set at the open boundaries (Fig. 2). A no-slip condition is set at the needle and the liquid-air interface. The mesh size around the stagnation zone is set to 1μm. Table 1 shows the parameters used in the simulation.

The simulation was done iteratively, starting at low pressure difference ΔP and upon increase of ΔP, the previous solution was used as an initial condition for the new simulation.

3.2 The thin film model

In a small slope approximation, the time evolution of the film thickness h on a solid substrate is given by the lubrication equation

(Oron 1997), which in cylindrical coordinates can be written as

$$\frac{\partial h}{\partial t} + \frac{1}{r}\frac{\partial}{\partial r} r \left(\frac{h^2}{2\mu}\tau_{jet} - \frac{h^3}{3\mu}\frac{\partial p}{\partial r} \right) = 0 \qquad (1)$$

and in which

$$p \equiv -\frac{\gamma}{r}\frac{\partial}{\partial r}\left(r \frac{\partial h}{\partial r} \right) + \rho g h - \Pi(h) + \Delta P_{jet} \qquad (2)$$

is the total pressure, μ is the viscosity, ρ is the density and γ is the surface tension. The disjoining pressure $\Pi(h)$ describes the effective pressure arising from interactions such as Van der Waals forces and electrostatic interactions. As a model disjoining pressure we use (Schwartz and Eley 1998)

$$\Pi(h) = B\frac{(n-1)(m-1)}{(n-m)h^*}\left[\left(\frac{h^*}{h}\right)^n - \left(\frac{h^*}{h}\right)^m \right] \qquad (3)$$

where $B=\gamma(1-\cos\theta)$. Here, θ is the equilibrium contact angle and h^* is a lengthscale of typically a few nanometers at which $\Pi(h=h^*)=0$. The integers $n>m>0$ influence the range of the interactions. The values used are listed in Table 2.

Initial film thickness	h_0	8μm
Surface tension	γ	45.4 mN/m
Viscosity	μ	49 mPa·s
Density	ρ	1125 kg/m^3
Contact angle	θ	5°
Parameters for Π	n,m,h^*	3, 2, 10 nm

Table 2: *Parameter values used for the simulation of a thin 3EG film on a partially wetting substrate.*

The interaction with the air-jet is modeled through the pressure profile $\Delta P_{jet}(r)$ and shear stress distribution $\tau_{jet}(r)$, that are obtained from numerical solution of the air-jet model.

As an initial condition we consider a flat film of thickness h_0. Furthermore, we prescribe $\nabla h=0$ and $\nabla p=0$ at $r=0$ and the boundary of the computational domain ($r=R_\infty$).

The domain size was taken to be $R_\infty=2$cm with mesh size 1μm around $r=0$ and 10μm for r>2mm. Simulations were performed using the commercial finite element software COMSOL 3.5a.

4. Results and Discussion

4.1 Air-jet simulation results

The air-jet simulations were performed up to an input pressure ΔP of 10 kPa. The center exit velocity at $\Delta P=10$ kPa is 87.5 m/s, the Reynolds number Re=587 and Mach number Ma=0.26, which is still in the laminar and incompressible regime. Figure 3a shows a typical profile of the pressure $\Delta P_{jet}(r)$ and shear stress $\tau_{jet}(r)=\mu du/dz$ at the sample position ($z=h_0$). The maximum values of stagnation pressure and shear stress normalized by ΔP are shown in Fig. 3b.
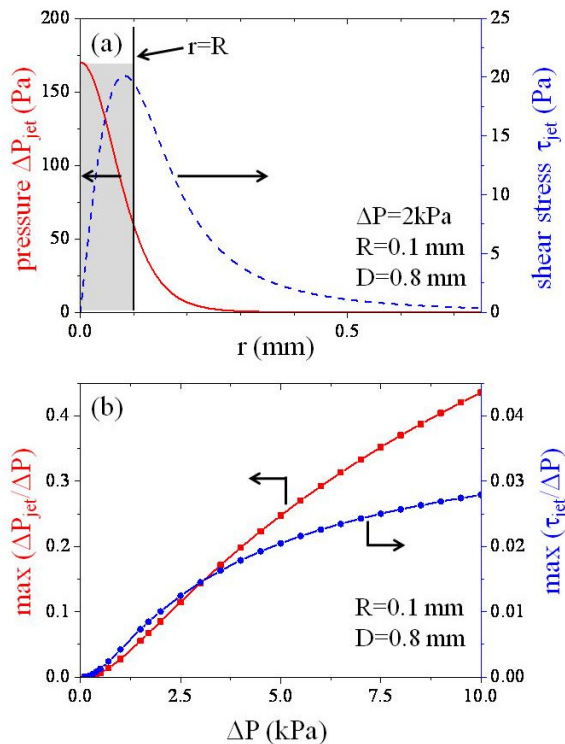
Figure 3: *(a) The pressure $\Delta P_{jet}(r)$ (red, left axis) and shear stress $\tau_{jet}(r)$ (dashed blue line, right axis) numerically calculated for $\Delta P=2$ kPa. (b) The normalized maximum values of ΔP_{jet} (red squares, left axis) and shear stress τ_{jet} (blue circles, right axis) as a function of ΔP.*

## 4.2 Air-jet impingement on a wetting film

In order to simulate the influence of an air-jet on a wetting substrate, the constants of Table 1 are used with the exception of the contact angle which is set to $\theta=0°$ and thus eliminating the disjoining pressure term. $\Delta P_{jet}(r)$ and $\tau_{jet}(r)$ were imported from the air-jet simulation and interpolated to fit to the mesh of the thin-film

model. The air-jet was active during 100s and turned off after that. Figure 4 shows some examples of the numerically calculated time evolution of the film height profile.
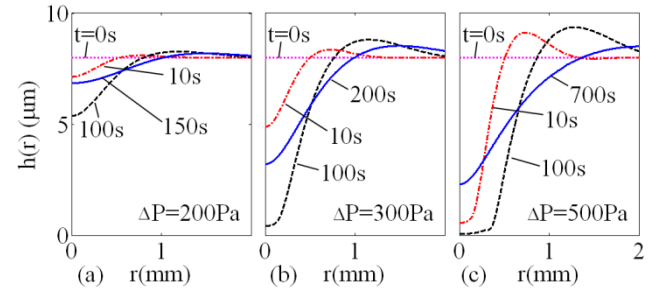
Figure 4: *Film height profiles as a function of time for a wetting film ($h_0=8\mu m$) subject to an air-jet pulse of duration 100s for (a) $\Delta P=200Pa$, (b) $\Delta P=300Pa$ and (c) $\Delta P=500Pa$.*

A dip is created that has a relatively flat center profile for higher values of input pressure ΔP. After the end of the pulse (t=100s) the film levels out again.
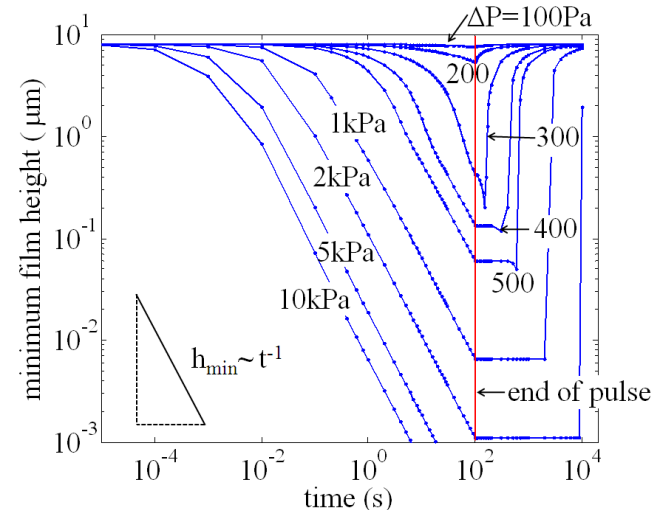
Figure 5: *Time evolution of the minimum value of the height profile (h_{min}) of a wetting film subjected to an air-jet for 100s at different ΔP.*

The minimum value of the height profile h_{min} as a function of time is shown in Fig. 5 for selected values of ΔP. After 100s the film stabilizes and the dip is filled up again. For high pressure settings $\Delta P>2$ kPa, the film is thinned to a value of 1nm or lower and refilling of the dip takes over 1000s. All curves appear to have the same asymptotic behaviour at low film thicknesses, where to good approximation $h_{min}{\sim}t^{-1}$. This agrees with

the results of Darhuber and Troian (Darhuber, in preparation) for the case of thinning films by shear stresses of thermocapillary origin.

Figures 6a, b and c show experimental results for the evolution of a 3EG thin film as a function of time for wetting films of 3EG on glass, subjected to an impinging air-jet for 100s.

For the air-jet with $\Delta P=500Pa$, an approximately 600nm deep dip is formed that levels out when the jet is switched off. An air-jet of $\Delta P=1.5$ kPa is enough to create a steep slope around a more or less flat center region of diameter approximately twice the needle diameter. After the jet is switched off, the film slowly moves back towards the center and fills the dip. During this leveling process the slope is reduced and fringes can be distinguished, indicating a dip depth of around 5.6μm.

At $\Delta P=10kPa$, a thin film with a non-uniform thickness is quickly formed. Over time the center area film thickness becomes uniform. After the air-jet is turned off, the film slowly refills the gap thereby showing fingering instabilities. These instabilities may originate from water uptake or trace amounts of contaminants in the liquid.

Comparing experiments and simulations, it is seen that the simulated dip for $\Delta P=500Pa$ is deeper than the experimental dip. This could be a sign that the air-jet strength was overestimated. Also the leveling dynamics of the film after the jet has been switched off is slower in the simulation than in experiments. Moreover, the thickness non-uniformities seen experimentally at higher ΔP and short times have not been reproduced in the axisymmetric simulations.
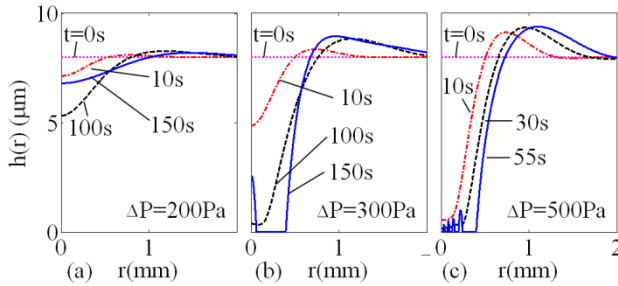
4.2 Air-jet impingement on a partially wetting film

Figure 7 shows an example of the time evolution of the film height profile for a partially wetting film subjected to an air-jet for 100s. All parameters except for contact angle $\theta=5°$ were identical to those used for Fig. 4. For $\Delta P=200Pa$, the height profiles are almost identical to the ones shown in Fig. 4a. At $\Delta P=300Pa$, the film ruptures after the end of the air-jet pulse and starts to dewet, leaving a
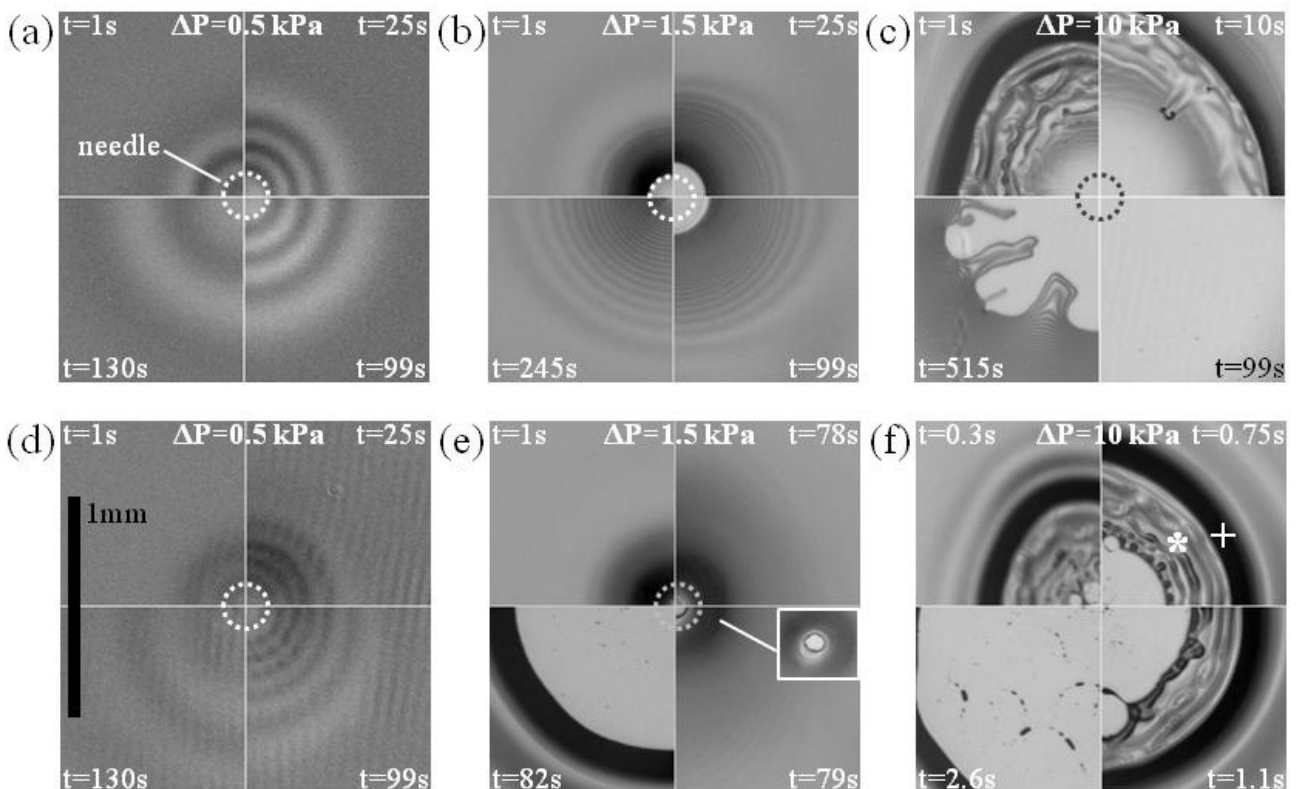
**Figure 6:** *The impact of an air-jet pulse from a hollow needle (Ø200μm, duration 100s) onto (a,b,c) a wetting film of 3EG on glass (6-8 μm) and (d,e,f) a partially wetting film of 3EG on PMMA at different pressure settings and different times during and after the jet.*

droplet at r=0 (a result of off-center rupture in an axisymmetric model). At higher pressure (Fig. 7c) the thin film in the center area has ruptured at multiple locations and dewetted before the end of the air-jet pulse.

Figure 7: *Film height profiles as a function of time for a partially wetting 8µm wetting film under a 100s air-jet pulse for (a) ΔP=200Pa, (b) ΔP=300Pa and (c) ΔP=500Pa.*
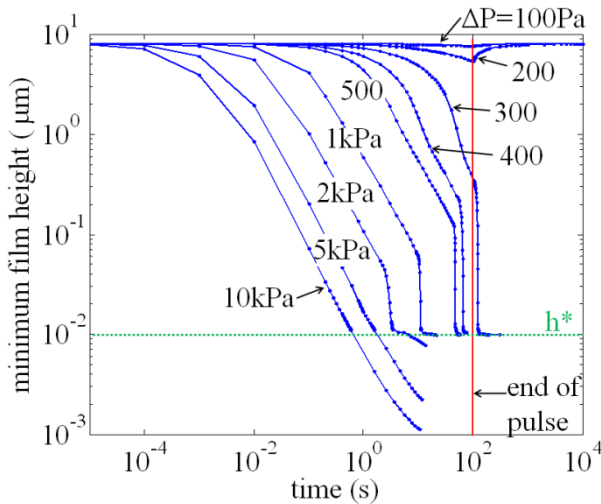
Figure 8: *Time evolution of the minimum value of the height profile of a partially wetting film subjected to an air-jet for 100s at different ΔP derived from numerical simulations.*

The minimum value of the height profile as a function of time for selected values of ΔP is shown in Fig. 9. After the end of air-jet pulse at t=100s the film stabilizes and the dip is filled up again for ΔP≤200Pa. For pressure settings ΔP>300 Pa, film rupture is seen. The time required for dry-spot nucleation varies from 125s to 0.6s depending on ΔP.

Figures 6d, e and f show the experimental results for the evolution of a thin 3EG film as a function of time for partially wetting films of 3EG on PMMA, subjected to an impinging air-

jet for 100s. It is seen that an air-jet with ΔP=500Pa impinging onto a partially wetting 3EG film, creates a dip of equal magnitude as for completely wetting surfaces and levels again.

The ΔP=1.5 kPa air-jet gives a dip with a steep slope, but a flat central area like the one observed in the wetting case is not seen. Counting interference fringes leads to conclusion that the film thickness is a few microns higher than the value measured immediately after spincoating. Film rupture occurs after 75±3s.

In the case of ΔP=10 kPa, a thin non-uniform film is created in the center area, which ruptures at multiple locations. Each dry-spot grows until the thin central film is merged into a common rim that grows radially. After dewetting, a pattern of droplets is left on the surface, indicating the positions where the rims of the initial dry-spots had coalesced.
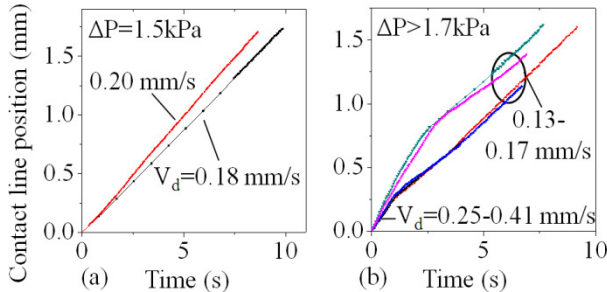
Both the experiments and numerical simulations show that for low ΔP, leveling occurs in partially wetting thin films. At intermediate pressures a single rupture site is seen, whereas at higher ΔP, a flat dip is created in which multiple dry-spots nucleate. Quantitative agreement between experiments and simulations requires an accurate expression of the disjoining pressure Π.

4.3 Dewetting speed

When the position of the dewetting contact line (the transition from dry-spot to liquid film) is tracked as a function of time, a dewetting speed can be extracted.

Figure 9 shows the contact line motion graphs that were extracted from several experiments. In the case of ΔP=1.5kPa, where only one dry spot is formed, the graph is a straight line and the dewetting speed V_d=0.18±0.02 mm/s is constant (Fig. 9a). For higher ΔP, the dewetting speed does not appear to be a constant (Fig. 9b). In the thinner center area (indicated by '*' in Fig. 6f), the dry-spots grow faster V_d=0.3±0.1mm/s until the common rim (indicated by '+' in Fig. 6f) is reached and at that point the dewetting speed decreases to a lower value V_d=0.15±0.02 mm/s. This qualitative behaviour is confirmed by a

numerical simulation, in which a step in film thickness was used as an initial condition and dewetting film profiles were calculated in the absence of ΔP_{jet} or τ_{jet} (Fig. 10).

Figure 9: *Experimentally determined position of the contact line as a function of time for the case of (a) a single rupture site (ΔP=1.5 kPa) and (b) for the case of a thin center layer with multiple rupture sites (ΔP>1.7 kPa).*
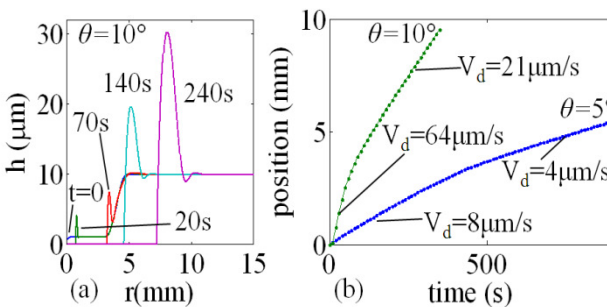
Figure 10: *Numerical simulation of the dewetting of a film with a step in film thickness. (a) height profiles for different times (b) contact line position as a function of time for two different contact angles θ .*

This appears to be contradictory to earlier observations (Brochard Wyart 1990 and Callegari 2002), in which the dewetting speed is predicted to be independent of thickness except in the regime where gravity becomes significant. In a recent paper the influence of film thickness and rim width was incorporated (Snoeijer 2010), which improves the agreement with the change in dewetting speed observed in our experiments and simulations. Quantitative agreement with our observations may be obtained by considering the presence of the shear stress from the air-jet, gravity and contact angle hysteresis.

5. Conclusions

The behaviour of a thin liquid film in the presence of an axisymmetric laminar air-jet has been studied experimentally and numerically. Stagnation pressure and shear stresses from the air-jet have been calculated numerically and used in a thin film model based on the lubrication approximation. Experiments with wetting and partially wetting films of triethylene glycol have been performed and the formation of depressions and dry-spots has been observed. For low-pressure air-jets, a dip is formed in the film that is filled again when the jet is turned off. In the intermediate regime a dry-spot can be triggered in a partially wetting film that grows with constant dewetting speed. At higher pressures, the film is thinned and ruptures at multiple locations, leaving a droplet pattern behind. Higher dewetting speeds were measured in the thin center area than in the surrounding liquid film, which was also seen in numerical simulations.

Simulations and experiments show qualitative agreement, but more accurate information on the disjoining pressure is needed to improve the agreement. Also, the air-jet calculations seem to overestimate the stagnation pressure and may need further refinement.

6. Acknowledgements

5. References

Banks, R.B. and Chandrasekhara, D.V., 1963. Experimental investigation of the penetration of a high-velocity gas jet through a liquid surface. J. Fluid. Mech. 15, 13-34.

Bower, C.L., Simister, A.E., Bonnist, E., Paul, K., Pightling, N. and Blake, T.D., 2007. Continuous Coating of Discrete Areas of a Flexible Web. AIChE J. 52, 1644-1657.

Brochard Wyart, F., Daillant, J., 1990. Drying of solids wetted by thin liquid films. Can. J. Phys. 68, 1084-1088.

Callegari, G., Calvo, A. and Hulin, J.P., 2002. Experimental results of dewetting in the visco-gravitational regime. Coll. Surf. A. 206, 167-177.

Collins, R.D. and Lubanska, H., 1954. The depression of liquid surfaces by gas jets. Brit. J. App. Phys. 5, 22-26.

Darhuber,A.A, and Troian, S.M.,
in preparation.

Ellen, C.H., Tu, C.V., 1984. Jet Stripping of Molten Metallic Coatings. Phys. Fluids. 28, 1202-1203.

Fagela-Alabastro E, Hellums JD, 1967. Laminar Gas Jet Impinging on an Infinite Liquid Surface. Ind. & Eng. Chem. Fund. 6, 580-587.

Fogt, N., King-Smith P.E., Tuell, G., 1998. Interferometric measurement of tear film thickness by use of spectral oscillations. J. Opt. Soc. Am. A 15, 268-275.

Holly, F.J., 1973. Formation and Rupture of the Tear Film. Exp. Eye Res. 15, 515-525.

Lacanette, D., Gosset, A., Vincent, S., Buchlin, J-M, Arquis, E., 2006. Macroscopic Analysis of Gas-Jet Wiping: Numerical Simulation and Experimental Approach. Phys. Fluids. 18, 042103.

Oron, A., Davis S.H. and Bankoff, S.G., 1997. Long-scale evolution of thin liquid films. Rev. Mod. Phys. 69, 931- 980.

Redon, C., Brochard, F. and Rondelez, F., 1991. Dynamics of Dewetting. Phys. Rev. Lett. 66, 715-719.

Reiter, G., 1992. Dewetting of Thin Polymer Films. Phys. Rev. Lett. 68, 75-80.

Schwartz, L.W. and Eley, R.R., 1998. Simulation of Droplet Motion on Low-Energy and Heterogeneous Surfaces. J. Colloid Interface Sci. 202, 173-188.

Sharma, A. and Ruckenstein, E., 1986. Finite-Amplitude Instability of Thin Free and Wetting Films: Prediction of Lifetimes. Langmuir 2,480-494.

Snoeijer, J.H. and Eggers, J., 2010. Asympotic Analysis of the Dewetting Rim. Phys. Rev. E 82, 056314.

Streefkerk, B., Mulkens, J., Moerman, R., Stavenga, M., Hoeven, J vd., Grouwstra, C., Bruls, R., Leenders, M., Wang, S., Dommelen, Y. v., Jansen, H., Cummings, K., Riepen, M., Boom, H., Suddenhof, M., Huisman, P., 2006. A dive into clear water: Immersion Defect Capabilities. Proc. SPIE 6154, 61540S.

Taylor, G.I. and Michael, D.H., 1973. On making holes in a sheet of fluid. J. Fluid Mech. 58, 625-639.

Tuck, E.O., 1983. Continuous Coating With Gravity and Jet Stripping. Phys. Fluids. 26, 2352-2358.